Supplementary information for "A near-quantum-limited diamond maser amplifier operating at millikelvin temperatures"

Morihiro Ohta[1], Ching-Ping Lee[2,8], Vincent P.M. Sietses[1,9], I. Kostylev[2], J.R. Ball[3,10], P. Moroshkin[3,11], T. Hamamoto[1], Y. Kobayashi[4], S. Onoda[5], T. Ohshima[5,6], J. Isoya[7], Hiroki Takahashi[1], Yuimaru Kubo[2*]

[1]Experimental Quantum Information Physics Unit, Okinawa Institute of Science and Technology Graduate University, Onna, Okinawa, 904-0495, Japan.
[2]The Science and Technology Group, Okinawa Institute of Science and Technology Graduate University, Onna, Okinawa, 904-0495, Japan.
[3]Quantum Dynamics Unit, Okinawa Institute of Science and Technology Graduate University, Onna, Okinawa, 904-0495, Japan.
[4]Sumitomo Electric Industries Ltd., Itami, Hyogo, 664-0016, Japan.
[5]Quantum Materials and Applications Research Center, Takasaki Institute for Advanced Quantum Science, National Institutes for Quantum Science and Technology, Takasaki, Gunma, 370-1292, Japan.
[6]Department of Materials Science, Tohoku University, Sendai, Miyagi, 980-8579, Japan.
[7]Graduate School of Pure and Applied Sciences, University of Tsukuba, Tsukuba, Ibaraki, 305-8550, Japan.
[8]Present address: Department of Physics, National Tsing Hua University, Hsinchu, 30013, Taiwan.
[9]Present address: QuTech and Kavli Institute of Nanoscience, Delft University of Technology, Delft, 2600 GA, Netherlands.
[10]Present address:, Liquid Instruments, San Diego, CA, 92130, USA.
[11]Present address: School of Engineering, Brown University, Providence, RI, 02912, USA.

1 Supplementary Methods

1.1 Cryogenic and room temperature setups

In this section, we describe the wiring and setup both inside the dilution refrigerator and at room temperature.

1.1.1 Wiring configuration in the dilution refrigerator

The detailed wiring and configuration inside the dilution refrigerator (Bluefors, LD-400) are illustrated in Fig. S1. Cryogenic attenuators (XMA, 2082-624X-CRYO series), represented as gray round rectangles, are inserted in each input line at every temperature stage to attenuate thermal noise from the microwave tone injected from room temperature. The heavily attenuated "Probe" line and moderately attenuated "Pump" line are combined at a directional coupler (Marki Microwave, C20-0226) on the mixing chamber stage. The labels "LPF" and "IRF" represent low-pass filters (Marki Microwave, FLP-0750) and homemade infrared filters using iron-loaded epoxy Eccosorb CR110, respectively. A HEMT (High Electron Mobility Transistor) amplifier (Low Noise Factory, LNA-LNC4_8C) was installed on the 4 K plate.

The calibrated noise source [1] is used for the noise temperature measurements. While the noise temperature is heated maximally up to ≈ 4.5 K, the base temperature of the mixing chamber plate slightly increases up to ≈ 19 mK.

Two microwave switches (Radiall, R573423600) were used to check the total attenuation of the coaxial cables to and from the noise source, which turned out to be negligible. The microwave switch (Analog Devices Inc., HMC547ALP3E), depicted inside the dashed box in Fig. S1, was installed and used only for pulse electron spin resonance (pulse-ESR) measurements to protect the HEMT. Further details are described in Sec . 2.1.

1.1.2 Pump cancellation

The probe tone was fed into the fridge through the line labeled "Probe", while the pump tone was sent through the line "Pump". To minimize the impact of the pump tone on the HEMT and the following receiver circuits, a cancellation microwave tone was introduced through a dedicated microwave input line labeled "Cancellation" (see also Fig. S2). When operating the maser amplifier, a microwave tone was generated by a signal generator (PSG; Keysight Technologies, E8267D) for both pump and cancellation. This tone was then split by a power splitter (Mini-Circuits, ZC2PD-01263-S+), as shown in Fig. S2a. On one branch, the cancellation tone was adjusted using a voltage-controlled phase shifter (Qorvo, CMD297P34) and a voltage-controlled variable attenuator (Pulsar Microwave, AAT-22-479A/7S). The amplitude and phase of this cancellation tone were adjusted to destructively interfere with the reflected pump tone through a directional coupler placed after the two circulators (Quinstar, QCY-G040082AS), resulting in suppression of the pump power by at least 50 dB.

1.1.3 Setup for maser gain and noise temperature measurement

The reflection coefficient $r(\omega)$ of the resonator was measured using a vector network analyser (VNA; Keysight, N5230C). The data presented in Figs. 2f and 3a, b, and d in the main text were measured at a power of $-110\,\mathrm{dBm}$, corresponding to a mean intra-resonator photon number of approximately 10^6, which is sufficiently lower than the number of inverted spins, $\Delta N_{P1+} \approx 4 \times 10^{14}$, ensuring minimal impact on the spin saturation. Although this power level almost reaches the typical saturation power of traveling-wave parametric amplifiers [2], it remains well below the saturation power of our maser amplifier as discussed in Fig. 4c in the main text.

Noise power spectra were measured by a spectrum analyser (SPA; Keysight Technologies; N9010A). The output and input ports of the VNA are connected to the Probe and Output ports of the fridge via directional couplers (input: Pulsar Microwave, CS20-09-436/9; output: Marki, C10-0226). A signal generator (SG, Keysight Technologies, E8247C) generates a microwave probe tone during the signal-to-noise ratio (SNR) measurements, as presented in Fig. 4a.

1.1.4 Setup for compression measurement

Figure S1b displays the wiring configuration on the mixing chamber plate used to measure the 1 dB compression points, as presented in Fig. 4C in the main text. To ensure the HEMT and subsequent components were not saturated, we bypassed the HEMT using a microwave switch.

1.1.5 Setup for pulse electron spin resonance measurements

In the pulse ESR measurement detailed in Sec. 2.1, we use an FPGA-based integrated measurement system (Quantum Machines, OPX+) to generate pulse envelopes, control microwave switches, and detect spin echo signals. Gaussian-shaped pulse envelope signals, modulated at 100 MHz, are generated by the OPX arbitrary waveform generator (AWG). We use the single sideband modulation technique, where a baseband microwave tone ("LO" in Fig. S2b) is mixed with the pulse envelopes with an internal IQ mixer of the PSG. These pulses are subsequently amplified by a high-power amplifier (Cree, CMPA601C025F) and fed to the resonator through the "Pump" line. To minimize microwave leakage noise from the amplifier, a semiconductor-based microwave switch (Analog Devices Inc., ADRF5019-EVALZ) is installed immediately after the amplifier's output. Similarly, another semiconductor-based microwave switch (Analog Devices Inc., HMC547ALP3E) is installed to protect the HEMT amplifier from the pulses.

For echo signal detection, the signals from the output port of the refrigerator are amplified by a series of room-temperature amplifiers (B&Z Technologies, BZ-02000800-090826-182020, and Mini-Circuits, ZVA-183+) and then down-converted using an IQ mixer (Marki, IQ-0307L). The local oscillator (LO) tones are extracted from a portion of the PSG's locking signal (option HCC). After demodulation, the signals are passed through band-pass filters (Mini-Circuits, SBP-101+), and then amplified by a preamplifier (SRS, SR445A). Finally, they are detected by the OPX's digitizer, which processes the signals digitally for heterodyne detection.

2 Supplementary Discussion

2.1 Echo-detected field-sweep spectroscopy

To characterise the impurity spins in our diamond, specifically the "fast-relaxing spins," we conducted an echo-detected field-sweep (EDFS) measurement using the setup depicted in Fig. S2b, with the pulse sequence illustrated in Fig. S3a. A practical challenge arises from the "long relaxing spins", namely the P1 and NV^- centres, which exhibit very long relaxation times ranging from approximately $\sim 10^3$ to $\sim 10^4$ seconds. Additionally, the substantial quantity of these impurity spins may hinder the signals from the "fast-relaxing spins", which turned out to be about two orders of magnitude less abundant. To mitigate this, we first saturated the P1 and NV^- centres using a 200-ms-long saturation pulse with frequency modulation of ± 10 MHz centred at the resonator frequency of 6.788 GHz in this cooldown. This allowed us to primarily detect the spin echo signals from the "fast-relaxing spins". This approach also enabled optimal adjustment of the room temperature amplifier chain to utilize the full dynamic range of the digitizer. After a waiting time of $T_W = 100$ ms, the echo signal was detected using a Hahn-echo sequence consisting of $\pi/2$ and π pulses.

The results of the EDFS measurement are shown in Fig. S3b. Despite the saturation pulse, several peaks associated with the P1 and NV^- centres remain visible. This is attributed to imperfections in the saturation pulse and partial population recovery during the 100 ms wait time. Nevertheless, a distinct "broad shoulder" feature is observed, extending from around the $P1_-$ peak at approximately 245 mT to around 260 mT. We fitted the data with a sum of nine Lorentzian functions. These components are also indicated by short arrows at the top of Fig. S3b. The broad signal stemming from the "fast-relaxing spins" is represented by a solid red curve.

2.2 Characterization of "fast-relaxing spins"

We measured the longitudinal relaxation times T_1 of the "fast-relaxing spins" under constant magnetic fields ranging from 247 mT to 260 mT using the saturation recovery pulse sequence [3]. The results are shown in Fig. S3c and d. Near the transition of $P1_-$, the relaxation curves exhibit bi-exponential decays, as presented in the upper panel of Fig. S3c. In contrast, in the fields higher than 253 mT, the relaxation curves can be fitted by a single exponential decay (bottom panel of Fig. S3c). This is attributed to the cross-relaxation effects with the $P1_-$ transition and their ^{13}C hyperfine-coupled transition.

As noted in the main text, we have not been able to rigorously identify the specific spin species constituting the "fast-relaxing spins." Nevertheless, the evidence presented below suggests that these may be neutrally-charged nitrogen-vacancy (NV^0) centres. First, we measured T_1 of P1 centres in a type Ib yellow diamond, an as-grown HPHT sample purchased from Sumitomo Electric Industries, Ltd., containing approximately 50 to 100 ppm of P1 centres, at 10 mK. The results, displayed in Fig. S4b, show spin relaxation times exceeding 4×10^3 seconds in the short T_1, about four or five times longer than those measured in the sample used for the maser experiments as presented in Fig. S4a. Similarly, the longer T_1 also shows 5.2×10^4 and 4×10^4 seconds. These

imply that the electron irradiation, i.e., the introduction of vacancies into our diamond crystal, likely created the "fast-relaxing spins" that exhibit the broad spin distribution (Fig. S3b), subsequently impacting the transitions of P1 centres.

Vacancy clusters [4] initially appeared to be possible candidates. However, these defects typically exhibit spin transitions with much narrower linewidths (significantly less than 1 mT) at temperatures below 100 K [4], which stands in stark contrast to the broad transition observed for the fast-relaxing spins in our diamond crystal. On the other hand, similar to negatively-charged silicon-vacancy (SiV^-) centres [5], the spins of NV^0 centres are sensitive to crystal strain [6, 7]. Such strain becomes significant in diamond crystals containing defect concentrations exceeding ≈ 1 ppm [8, 9], which is indeed the case for the diamond crystal used in our experiments.

References

[1] Simbierowicz, S. *et al.* Characterizing cryogenic amplifiers with a matched temperature-variable noise source. *Review of Scientific Instruments* **92**, 034708 (2021). URL https://aip.scitation.org/doi/full/10.1063/5.0028951. Tex.ids= simbierowiczCharacterizingCryogenicAmplifiers2021a publisher: American Institute of Physics.

[2] Esposito, M., Ranadive, A., Planat, L. & Roch, N. Perspective on traveling wave microwave parametric amplifiers. *Applied Physics Letters* **119**, 120501 (2021). URL https://aip.scitation.org/doi/10.1063/5.0064892.

[3] Schweiger, A. & Jeschke, G. *Principles of Pulse Electron Paramagnetic Resonance* (Oxford University Press, Oxford, New York, 2001).

[4] Iakoubovskii, K. & Stesmans, A. Dominant paramagnetic centers in 17 O - implanted diamond. *Physical Review B* **66**, 045406 (2002). URL https://link.aps.org/doi/10.1103/PhysRevB.66.045406.

[5] Meesala, S. *et al.* Strain engineering of the silicon-vacancy center in diamond. *Physical Review B* **97**, 205444 (2018). URL https://link.aps.org/doi/10.1103/PhysRevB.97.205444. Publisher: American Physical Society.

[6] Baier, S. *et al.* Orbital and Spin Dynamics of Single Neutrally-Charged Nitrogen-Vacancy Centers in Diamond. *Physical Review Letters* **125**, 193601 (2020). URL https://link.aps.org/doi/10.1103/PhysRevLett.125.193601. Publisher: American Physical Society.

[7] Kurokawa, H. *et al.* Coherent electric field control of orbital state of a neutral nitrogen-vacancy center. *Nature Communications* **15**, 4039 (2024). URL https://www.nature.com/articles/s41467-024-47973-3. Publisher: Nature Publishing Group.

[8] Liu, A., Cundiff, S. T., Almeida, D. B. & Ulbricht, R. Spectral broadening and ultrafast dynamics of a nitrogen-vacancy center ensemble in diamond. *Materials for Quantum Technology* **1**, 025002 (2021). URL https://dx.doi.org/10.1088/2633-4356/abf330. Publisher: IOP Publishing.

[9] Acosta, V. M., Jensen, K., Santori, C., Budker, D. & Beausoleil, R. G. Electromagnetically Induced Transparency in a Diamond Spin Ensemble Enables All-Optical Electromagnetic Field Sensing. *Physical Review Letters* **110**, 213605 (2013). URL http://link.aps.org/doi/10.1103/PhysRevLett.110.213605.

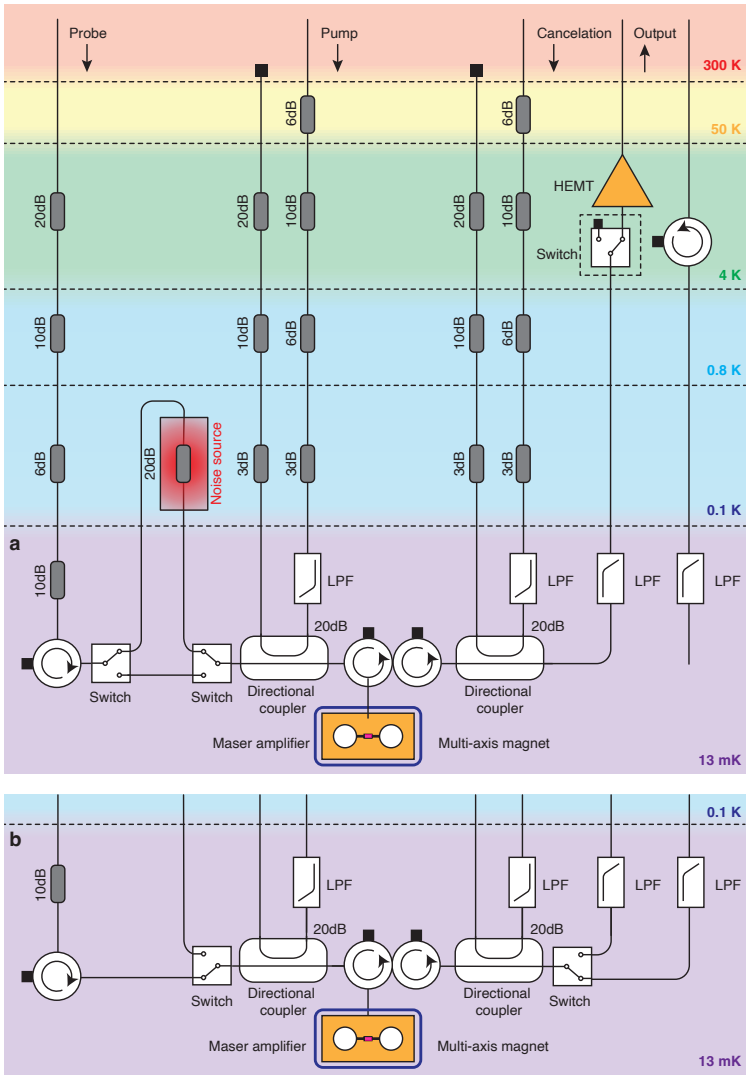

Fig. S1 Cryogenic wiring and configurations. "LPF" and "IRF" denote a 7.5 GHz low pass filter and an infrarad filter, respectively. The microwave switch located below the high-mobility transistor amplifier (HEMT) at 4 K is used only for pulse-ESR (electron spin resonance) measurements. The decibel numbers indicate the values of attenuators (gray round rectangular) and directional couplers. **a**, Setup at 13 mK for maser gain and noise temperature measurements. **b**, Setup at 13 mK for the saturation measurements. The right-side switch at 13 mK is used to bypass the HEMT during these measurements.

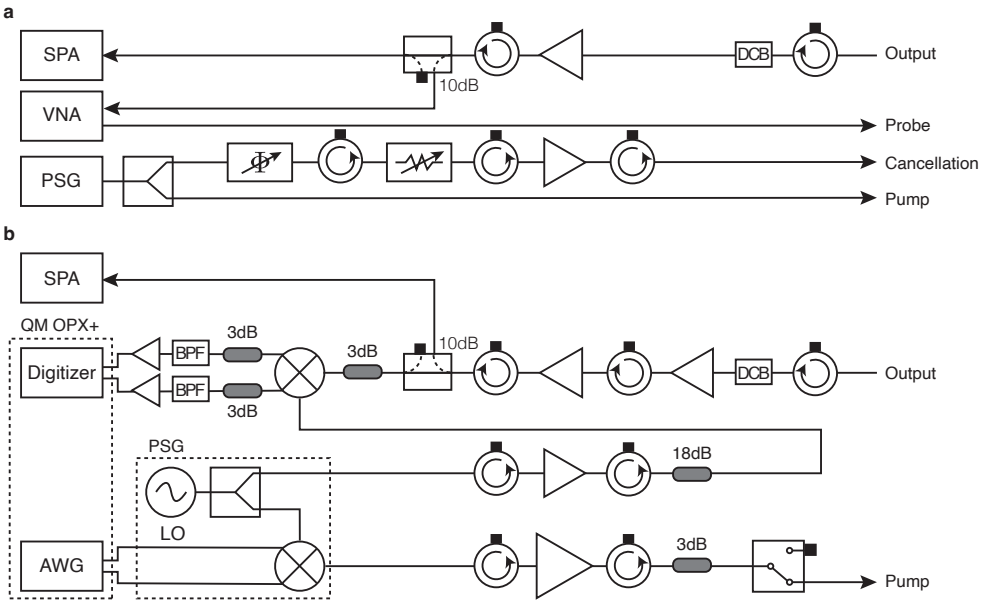

Fig. S2 Room temperature measurement setup. "BPF" and "DCB" denote a $94 - 108\,\mathrm{MHz}$ band pass filter and a DC block, respectively. (**A**) Setup for masing measurement. (**B**) Setup for pulse ESR measurement.

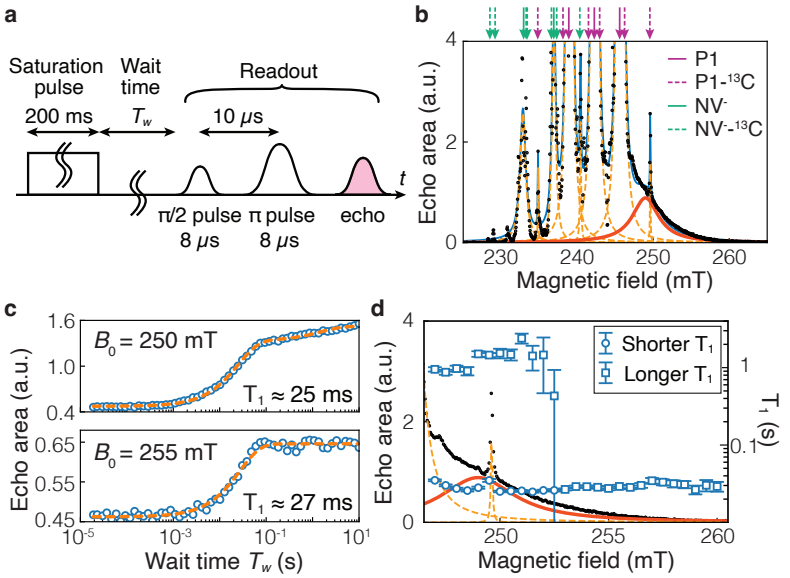

Fig. S3 Electron spin resonance spectroscopy and relaxation time measurements. a, Pulse sequence used for the echo-detected field-sweep (EDFS) spectroscopy and saturation recovery measurements. The wait time T_{W} was fixed at 100 ms for EDFS spectroscopy and was varied for T_1 measurements. **b**, EDFS signals as a function of the magnetic field. Black points depict experimental data, while the blue solid curve indicates the fit using nine Lorentzian functions. Orange dashed curves correspond to fitting results for known defects in diamond, i.e., P1 and NV^- centres, and their hyperfine transitions with $^{13}\mathrm{C}$ centres at the nearest neighbors. The red solid curve represents fast-relaxing spins. Calculated resonant magnetic field values for known defects are indicated by short arrows at the top. **c**, Results of saturation recovery measurements. Echo area as a function of wait time T_W at a magnetic field of $B_0 = 250\,\mathrm{mT}$ (upper panel) and $B_0 = 255\,\mathrm{mT}$ (lower panel) are plotted. Orange dashed lines show the result of bi-exponential fitting in the upper panel and single-exponential fitting in the lower panel. **d**, T_1 as a function of the magnetic field, with the EDFS spectroscopy data overlaid. Circular and square markers represent the shorter and longer T_1 components obtained from bi-exponential fits. Data obtained above 253 mT can be fitted with a single exponential.

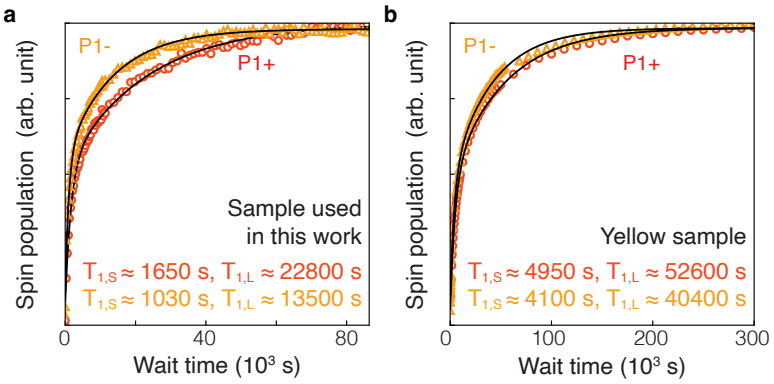

Fig. S4 Spin relaxation measurements of two different diamond samples. a, Results of the sample used in this work. The data were fitted using a bi-exponential function, and the two relaxation times, i.e., the shorter $T_{1,\mathrm{S}}$ and longer $T_{1,\mathrm{L}}$, are displayed. **b**, Results of a yellow diamond sample.